The Global Zonally Integrated Ocean Circulation (MOC), 1992-2006: Seasonal and Decadal Variability

Carl Wunsch and Patrick Heimbach
Department of Earth, Atmospheric and Planetary Sciences
Massachusetts Institute of Technology
Cambridge MA 02139 USA
email: cwunsch@mit.edu, heimbach@mit.edu

March 1, 2008

Abstract

The zonally integrated meridional and vertical velocities as well as the enthalpy flux in a least-squares adjusted general circulation model is used to estimate the oceanic meridional overturning (MOC) and its variability, 1992-2006. A variety of simple theories all predict that the mid- and high-latitude oceans should respond to atmospheric driving only on multidecadal time scales and, in practice, little change is seen in the MOC and associated heat transport except right at the sea surface, at depth near the equator, and in parts of the Southern Ocean. Variability in meridional transports in both volume and enthalpy is dominated by the annual cycle and secondarily by the semi-annual cycle, particularly in the Southern Ocean. Although the estimates show a net uptake of heat from the atmosphere (forced by the NCEP-NCAR reanalysis which produces net ocean heating), no significant trends are found in meridional transport properties over 15 years.

1 Introduction

The North Atlantic meridional overturning circulation (NA-MOC) has been the focus of intense interest, in part because of widely publicized claims that it controls much of the climate system, or is in imminent danger of "collapse" or both. A number of studies (e.g., Hurrell et al., 2006) have discussed predicting the NA-MOC under the presumption that it is a dominant component of ongoing climate change. Wunsch and Heimbach (2006) discussed the behavior of the MOC in the Atlantic at 25°N between 1993 and 2004, concluding that there were weak trends at various depths in the meridional volume transport, but that there was no evidence for a significant trend in the heat (temperature) transport.

But the NA-MOC is part of the global ocean circulation and can only be understood in the global context. Here we examine the planetary zonally integrated meridional ocean circulation as computed from a combined oceanic GCM and the large data sets in the ECCO-GODAE estimates (see Wunsch and Heimbach, 2007, for a complete description, and Wunsch and Heimbach, 2006, for its North Atlantic behavior; the acronyms represent Estimating the Circulation and Climate of the Ocean, and Global Ocean Data Assimilation Experiment) and analyze its mean and variability over the 14 year period 1992-2006. There are no eddies present in this 1° horizontal, 23-vertical layer representation and thus the variability is a lower-bound (e.g., Wunsch, 2008). The specific solution is denoted v3.22 and differs quantitatively in numerous ways from the unoptimized control run (v3.0) which represented the starting estimate. A brief description of the v3.22 ECCO-GODAE estimate is that is the result of a least-squares fit of a general circulation model (GCM) to a global, weighted data set, 1992-2004. Comparisons (not shown) of the equivalent results in the "control" solution obtained by forcing the MITgcm with the unmodified NCEP-NCAR reanalysis in the configuration discussed by Heimbach (2008, in preparation) lead to the inference that changes in the circulation required by the optimization are quantitative rather than qualitative, the variability structure remaining largely the same. An exception to this statement is that the mean Atlantic MOC is qualitatively shifted in magnitude. Comparisons (not shown) to an earlier near-optimized solution (v2.216) show very similar results.

Discussion of almost any aspect of the global ocean circulation runs the risk of extending to book-length. The shorthand "MOC" is convenient, but fundamentally, we are examining the zonal projection of a three-dimensional flow field. Use of zonally integrated quantities in geographical coordinates, has the advantage of simplifying the results and making their display reasonably straightforward. It has the disadvantage of precluding analysis of the three-dimensional flow and transport fields producing the integrated results—no two-dimensional projection can provide full information about a three-dimensional flow. Seeming paradoxes can arise from such projections if they are interpreted as representing particle pathways. These disadvantages are set aside for the time-being in an effort to produce a comprehensible, simple, description of the ocean circulation variability—a description that has been widely invoked to discuss the present, past and future climate states. Recalculation of the results in e.g., neutral density space, and in the Southern Ocean, in stream-coordinates as the residual mean, would be illuminating, but again these are not displayed here. In our present useage, "MOC" refers to the top-to-bottom circulation; some other authors employ the term for the very-near-surface, highly volatile flow, and which for this paper, is regarded as a separate subject.

Before analyzing the estimated results, it is useful to recall the venerable (Veronis and

Stommel, 1956) and well-supported theory (Gill, 1982; Pedlosky, 2003; Cessi et al., 2004) of ocean response to disturbances. One expects the baroclinic oceanic response to perturbations to be governed in large part by the zonal propagation of signals by baroclinic Rossby waves. At mid-latitudes, the group velocity of such a wave requires on the order of a decade to propagate a signal across a 5000km wide ocean, with the time growing substantially at higher latitudes (see also, Sturges et al., 1998). The inability of the subtropical and higher latitude oceans to respond baroclinically at annual periods is the basis of the Gill and Niiler (1973) depiction of the seasonal variability as essentially local except at low latitudes, an inference that has stood the test of time. (Barotropic adjustment is much faster.)

Fig. 1 displays the time required for the baroclinic Rossby wave with the fastest group velocity to cross a 5000km wide ocean as a function of latitude. The fastest wave is, in the basic theory, the one with the basin-scale wavelength. The multi-decadal time scale in the modeling results of Cessi, et al. (2004) are fully consistent with expectation. These times (and basin widths do change with latitude) are not the adjustment time—they are the shortest time over which baroclinic adjustment can be expected to *start*.[1] Such time scales are the result of linear perturbation theory and would not necessarily be applicable in a situation where the ocean was subject to a major finite amplitude disturbance. A question raised below is whether there is any evidence the ocean is, in modern times, being subjected to sufficiently large disturbances that the simple theory is rendered invalid. Anticipating the conclusions, results are consistent with the rough temporal scaling argument embodied in Fig. 1 and the inference that over the last 15 years, disturbances lie well within the small perturbation range. The Southern Ocean is a partial exception to the conclusions about time scales.

Convective injection of surface waters into the abyss at high latitudes might be thought to short-circuit the baroclinic wave adjustment time. Consider, however, that convective regions are by nature extremely small, and while communication between surface and abyss is locally fast, the ability to adjust large fractions of the abyssal ocean will again depend upon the wave-signal velocities, or even slower advective ones carrying information away from the convective area. By way of example, consider that the North Atlantic volume between 50°N and 80°N is about 1.5×10^{16} m^3. If the change in convective injection of surface water were as large as 10Sv (an extremely large value), and if the entire convected volume were restricted to that region (physically impossible), then the time to replace the water mass would be about 50 years. Large integrated variability in the deep oceans on a decadal time scale are not expected—with implications both for predictability and near-term detectability.

[1] Baroclinic Kelvin waves—coastal and equatorial—are much faster, but influence the ocean interior only indirectly through their coupling to Rossby waves when reflecting and shifting latitude.

Oceanic potential energy is

$$PE = \iint \int_{-h(\lambda,\phi)}^{\eta(\lambda,\phi)} zg\rho\,(\lambda,\phi,z)\,dzdA$$

with g gravity, ρ density, ϕ longitude, z the vertical coordinate, dA the area differential, h the depth and η the sea surface elevation. In a linear approximation, $\rho = \rho_0\,(1-\alpha T+\beta S)$, with T being temperature, S salinity and $\rho_0 \approx 1029\mathrm{kg/m}^3$. In the modern ocean (e.g. Oort et al., 1989), $PE \approx 10^{26}$J and any major disturbance to the circulation would modify this reservoir. Estimates of energy transfers to the ocean circulation from the atmosphere are today of order 1TW (10^{12}W). Keeping everything else fixed, suppose, to derive a time-scale, the ocean below 1000m undergoes a temperature change (either sign) of 1°C. Then,

$$\Delta PE \approx g\rho_0 \iint \int_{-h(\lambda,\phi)}^{-1000\mathrm{m}} (-\alpha\Delta T)\,zdzdA \approx 10^{22}\mathrm{J}$$

(using $\alpha \approx 1.7\times 10^{-4}/°\mathrm{C}$ and $h \approx -4000$m).

Cooling of the abyss lowers the center of mass implies a reduction in PE, and which could be released as kinetic energy or transferred through the sea surface; correspondingly a warming represents an increase in PE, which could derive from mixing forced by oceanic kinetic energy or, again by transfer across the sea surface. If the modern rate of energy input of order 1TW were to be disturbed by 100%, then it would take about 300 years to bring about an energy shift of this magnitude. (Estimated modern conversion rates between PE and KE are less than 1TW; see Ferrari and Wunsch, 2009.) Qualitative shifts in the circulation potential energy would require *multi-decadal* periods unless the energy transfer rates both within the ocean and to and from the atmosphere, were greatly modified from present-day value—implying a significant shift in the way existing air-sea coupling occurs. Equivalent calculations can be made for salinity (fresh water input) changes, and we are ignoring corresponding changes in internal and kinetic energy.

Conventionally, the MOC is displayed as a stream function in latitude, ϕ, and vertical, z, coordinates (see e.g., Talley, 2003; Lumpkin and Speer, 2007), but that representation seems no more visually informative than one in the two components, v, w, of the Eulerian velocities. For each ocean basin, including the Southern, the meridional velocity, v, is integrated zonally to produce e.g., $V_i\,(\phi, z, t)$, where i is used to denote the results in each of the four basins, Atlantic, Pacific, Indian, and Southern and time means $\bar{V}_i\,(\phi,z)$, $\bar{W}_i\,(\phi,z)$are formed. Another advantage of using v, w is that the Indian and Pacific Oceans can be depicted independently—use of a stream function requiring the summation of those basins. The model is defined at 1° intervals of latitude and longitude, between 79.5° north and south, and in 23 levels,[2] so that $\phi = \phi_j$,

[2] Layer interfaces are at: 0, 10, 20, 35, 55, 75, 100, 135, 185, 260, 360, 510, 710, 985, 1335, 1750, 2200, 2700, 3200, 3700, 4200, 4700, 5200, 5700 meters.

$z = z_k$ corresponding to integer values j, k (k defining the center of the layers). For context, we begin with a brief description of the time means, turning later to the variability. Ocean dynamics depend most directly on the mass (volume) flux, whereas the coupled atmosphere responds most immediately to the enthalpy (heat) transport and, particularly, the related sea surface temperature. Oceanic fresh water transport is also important, but in the interests of restricting the length of this discussion, we here omit any discussion of fresh water and salinity.

2 Mean Global Volume and Enthalpy (Heat) Transports

2.1 Volume Transport

Fig. 2 displays $\bar{V}_i(\phi, z)$, over the entire 15 years, for Atlantic, Pacific, Indian (all north of 38°S) as well as for the Southern Ocean. In gross terms, one sees an Atlantic with a conventional MOC, having a northward flow in the upper approximately 1000m, a southward flow between about 1000 and 4000m and generally northward flow below that. The color shifts across fixed depths imply vertical divergences necessary to conserve volume or mass. Ganachaud (2003) provided independent estimates of the zonal integrals at a few latitudes.

The Pacific is also as expected, with a surface outcropping of the southward flow in the northern hemisphere consistent with intermediate water formation, and penetration of water from the circumpolar area near surface and bottom, sandwiching a southward return flow at intermediate depths. The less familiar Indian Ocean is similar on average to the South Pacific. Dynamically, and also unsurprisingly, the Southern Ocean is quite different from the others, with intense meridional flow appearing only below the sill depths, and being dominated by inflow from the north, with intense northward flow being confined to great depths at low latitudes. An intricate cellular structure appears at depth on the equator in the Atlantic and Pacific Ocean, particularly in the latter. Results from the control run, v3.0, are grossly similar, but differ in many details, and are not displayed here.

Fig. 2 is a bit misleading in that the near-surface (and near-bottom) flows are quite intricate, as can be seen in Fig. 3 which is identical to Fig. 2 except showing an expanded upper 300m. The Pacific result has a strong qualitative resemblance between 8°S and 10°N to Fig. 5a of Johnson et al. (2001) who used shipboard ADCP data, not employed here, in displaying the near-surface divergence expected from Ekman layers, overlying a reversed sense flow below that to about 300m, with southward flow to about 100m on the equator itself. The Atlantic shows a similar, but weaker, structure. A more detailed discussion of the near-equatorial physics would, however, take us too far afield from a global account. The near-surface Southern Ocean displays a divergence about, very roughly, the mean latitude of the Antarctic Circumpolar Current with a strong equatorward Eulerian mean to the north of the axis—again as one would anticipate from Ekman theory. (The eddy volume flux must be accounted for there, should one seek to discuss particle motions.)

Much attention has gone toward determining the poleward volume flux, and Fig. 4 displays the maximum definable value (whether poleward or equatorward), obtained by integrating downward from the surface, in each ocean basin. Atlantic values near 15Sv are conventional.The control differs qualitatively, e.g. in the Atlantic, where the maximum meridional overturning increases with latitude from little more than 12Sv to more than 23 by about 50°N. For this component, the optimization has made an important change.

The vertical velocities associated with the divergences of the meridional flow in Fig. 2 are shown in Fig. 5. The patterns are not, globally, simple, but a number of familiar features do emerge, including the comparatively strong near-surface equatorial upwelling, a strong Deacon Cell in the Southern Ocean and a strong downwelling in the high latitude convective region of the North Atlantic. (See Scott and Marotzke, 2002, for a discussion of vertical velocities and convective mixing in idealized models.)

The flow pathways dictated by these time means are not our present focus. Nonetheless, some understanding of the basic time average pathways can be obtained from the long-term tracer experiments of Wunsch and Heimbach (2008), and/or the schematic of Lumpkin and Speer (2007), which appears qualitatively plausible.

2.2 Enthalpy Transport

The temperature transport primarily reflects the underlying volume transports. Fig. 6 displays the time-mean temperature transport (Indian and Pacific values need to be added for mass conservation if one is to discuss the heat transport there). As expected (see e.g., Boccaletti et al., 2005) the temperature weighting of the volume transport produces a strong near-surface amplification of the enthalpy transport, whose structure is readily inferred from Fig. 2 and 3. Its physics are dependent, however, upon the much deeper volume transports (that is, a disruption of the deeper meridional volume flux would change the near-surface temperature transports). Upper tropical layers are strongly divergent, as implied by Fig. 3.

3 Global Variability

Fig. 7 depicts the variance of $V(\phi, z, t)$ over 15 years in the solution (the standard deviation of the variability is 0.83Sv). Most of the variance at depth is, as expected, at low latitudes, with the exception of the deep Southern Ocean in the region of topographic structures. As will be seen below, the deep Southern Ocean change is dominated by a semi-annual component. See Webb and de Cuevas (2007) and Olbers and Lettmann (2007) for discussion of Southern Ocean variability.

3.1 Volume Transport Components

The analysis procedure is a standard one for empirical orthogonal functions (EOFs, e.g., Jolliffe, 2002; von Storch and Zwiers, 1999) although we prefer a slightly unconventional description using the singular value decomposition (Appendix 1). For each basin, a monthly anomaly of meridional transport is computed as $V_i'(\phi_j, z_k, t_p) = V_i(\phi_j, z_k, t_p) - \bar{V}_i(\phi_j, z_k)$ and the spatial EOFs, here called $\mathbf{u}_i$ computed with temporal coefficients, $\mathbf{v}_i(t)$, and singular value λ_i. As is always the case with EOFs, a choice about weighting has to be made; the fields could be given uniform variance, or normalized to represent zonal averages rather than integrals. Here the raw integrals represent the variables with the most immediate impact on the climate system: The resulting heavy weighting of the Pacific and Southern Oceans represents their enormous mass of fluid, and which at zero order, will control the air-sea transfer processes. Other weightings will produce results that differ, and their analysis likely would be enlightening.

The issue of trends and drifts is one of the more difficult ones in using GCMs, and we postpone that discussion. For the moment, note only that some, but by no means all, of the $\mathbf{v}_i(t)$ display starting transients ranging from a few months to 2+ years; the effect is particularly pronounced in the Atlantic basin and in particular, for the spectral results shown below, the first two years of the estimates were dropped in the Fourier analysis used to calculate power density estimates.

Figs. 8, 9 display the first two singular vectors (EOFs) of the volume flux containing 43% of the total volume variability $(0.83\ \mathrm{Sv})^2$ and 8% respectively of the total. Many more modes carry a slowly decreasing fraction of the variance. As with all EOFs here, they are computed globally—reflecting the global covariances, but are displayed by ocean basin for interpretation.

Three additional transport EOFs can be seen in Appendix 2, all having a few percentage of the transport variability variance. Two of them have a largely tropical and Southern Ocean *semi-annual* variability and the third shows a dominantly low frequency structure.

Contrary to what one might have anticipated from much of the literature, almost all of the MOC variability is annual and secondarily, semi-annual, and, from the annual cycle to the decade+ time scale, it is dominated by the Pacific Ocean with its immense expanse of low latitude, rapidly-responsive, volume; the Indian Ocean is a close second in importance. That much greater volatility appears at low latitudes is consistent with the theory sketched above. Although the ECCO-GODAE estimates are known to have high latitude convection that tends to penetrate too deeply owing to a failure to restratify rapidly enough, there is nonetheless only slight evidence for any annual variability at high latitudes from that effect. Many discussions exist of near-surface annual variability. Rabe et al. (2008), for example, discuss the near-surface annual cycle in the tropical Atlantic from a 50-year ECCO calculation, albeit data prior to 1993 are extremely thin. Keenlyside and Kleeman (2002) summarize some of the theoretical understanding of the top about 200m. The global decadal scale variability is not simple except insofar as it is dominated by low-latitude processes. Little or no high latitude variability is evident.

One, $\mathbf{v}_5(t)$, has a structure corresponding to a trend (see the Appendix 2). Other vectors have low frequency structures indistinguishable from red-noise processes observed over an interval too short to delineate the actual spectral form.

3.2 Temperature Variability

The time-mean temperature (and salinity) fields are visually conventional and so are not displayed. Figures 10-11 show the first two EOFs of the zonally integrated temperature fields. The first EOF is the major exception to the absence of simple global trends, showing a nearly linear trend in temperature over the entire calculated history. It corresponds to a general warming of the Atlantic, Pacific and Indian Ocean thermoclines with a corresponding cooling in the deeper levels of the Southern Ocean. We will discuss it below. Two more, predominantly semi-annual dominated, EOFs can be seen in Appendix 2.

3.3 Enthalpy Transports

Interpretation of the enthalpy (heat) transports requires a context for the magnitudes of the time-mean transports. Fig. 12 shows an estimate of the oceanic meridional heat transport (Wunsch, 2005) computed independently of the ECCO-GODAE estimates (primarily from Ganachaud and Wunsch, 2002). For comparison, the ECCO-GODAE result is shown in Fig. 13. Within error estimates, the global total is indistinguishable from that in Fig. 12, although it is closer to anti-symmetry about the equator. Because of the strong eddy transport in the Southern Ocean, the value shown there differs qualitatively from those obtained from an eddy-permitting model (M. Mazloff, private communication, 2008) or in the residual mean computed from the present model. In Mazloff's results, the eddy contribution (not shown here), is such as to remove much of the structure seen in Fig. 13, leading to a nearly linear increase in the total southward heat transport from south to north reaching about -0.4PW at the northern limit.

About 20 EOFs are required to reproduce 95% of the squared norm of the variability. As with the volume flux, dominant variability is at the annual and semi-annual periods and dominated by the tropical Indian and Pacific Oceans (Figs. 14, 15).

The third and fourth, semi-annual dominated EOFs are shown in Appendix 2. As noted for the North Atlantic by Wunsch and Heimbach (2007), the enthalpy transports display weaker apparent trends than do the volume fluxes, and to the degree that climate depends primarily on the former, there is no evidence after 15 years for any major shift occurring in the global ocean circulation with climate consequences. That the enthalpy flux is not dominated by the trend seen in the first temperature EOF is consistent with the North Atlantic inference of Wunsch and Heimbach (2006), that the system is dominated by the velocity variability, not that in temperature, which is lost in the noise level.

4 Ice Cover

Sea ice is an important component of the model at high latitudes, where observed ice-cover is part of the misfit function. Its temporal variability (not shown), is dominated by the Southern Ocean annual cycle with 92% of its temporal variance, and by the semi-annual (5% of the variance). Higher EOFs are nearly white noise and none of them suggests a sea ice-cover trend. Note, however, that this system version does not include the Arctic.

5 The Forcing

In the interests of comparative brevity, we discuss only the zonal wind component—much the stronger of the two. Time means of the meteorological forcing fields are not displayed here, as they are visually unsurprising—with e.g., bands of easterlies and westerlies in the wind. Variability within the ocean can be the result of direct forcing structures, but also arising from internal instabilities and free modes. Some insight can be gained by looking at the low EOFs of the forcing variables, with particular interest in any observed trends.

The first two EOFs of τ_x variability are shown in Figs. 16, 17. The first mode is essentially the annual variability and the second is that of a broad-band variability over the ACC (Drake Passage latitude) with a separate semi-annual peak. A strong semi-annual peak in Southern Ocean winds is well-known (e.g., Trenberth et al., 1989, or Meehl, 1991), as is another weak maximum in the North Pacific. The strong Southern Ocean variability in the second EOF is sufficiently narrow in latitude that estimates (e.g., Cunningham and Pavic, 2007) based upon atmospheric pressure differences between 45°S and 65°S would tend to miss the activity. A general discussion of atmospheric wind structures can be found in Thompson and Wallace, 2000 and Thompson et al., 2000).

The associated atmospheric heat fluxes to and from the ocean are shown in Figs. 18, 19. These are dominantly annual and semi-annual in nature, with the latter again being particularly conspicuous in the Southern Ocean, here straddling the ACC. None of the first 10 EOFs shows a visual trend, and evidently the atmospheric heating of the ocean is, unsurprisingly, a very small disturbance superimposed upon a very energetic system.

Huang et al. (2006) showed an apparent increase of 12% in the rate of working of the wind (as depicted by the NCEP-NCAR reanalysis) over the 25 years beginning in 1980. To the extent that there exist trends in the zonal wind stress in the shorter period used here, they are a complex sum of spatially complicated structures in the higher EOFs (not shown). None of the first 10 zonal wind EOFs show a simple visual trend.

A fundamental question is whether the meteorological disturbances applied to the ocean are sufficient to drive its response out of the range of the simple perturbation theory ideas invoked above? As we have seen, there is no particular evidence of long-term, large-scale trends that might be shifting the mean state, although surely low frequency variability on time scales longer than 15 years must be present. As a crude measure of the degree of disturbance, note that the space/time variance of the zonal stress is about 12% of the spatial variance of the mean field and includes the very strong annual cycle. There is no reason to believe that large-scale finite amplitude responses are present now.

The first two EOFs of the enthalpy transfer to the atmosphere have the same temporal structure as the wind field, but almost all of the variance is in the annual cycle with less than 1.5% in the semi-annual, which is again peaked over the Southern Ocean.

6 The Trends

Both the control and the present best-estimate, v3.22, have a temperature EOF corresponding to a large-scale uptake of heat near-surface almost everywhere at a rate of about 3.4W/m^2. This heating arises from the atmospheric state in the NCEP-NCAR reanalysis (Kalnay et al., 1996) and which is employed here using bulk formulas. The value may well be reduced with further optimization iterations, if it is incompatible with the in situ oceanic data. Thus far, however, there is no evidence that the oceanic data, within error bars, are in conflict with such a heat uptake—implying that the data remain too sparse and noisy to force a reduction in the atmospheric heat flux. Despite the presence of this uptake of heat, whether justified or not, it has little or no effect on the meridional transports of volume (mass) or heat, being lost in the overall noisiness of the system. The wind field has already been discussed.

Bindoff et al. (2007) describe evidence for trends, over several decades, in oceanic ventilation rates, through observations of such fields as the oxygen distribution. In the present 15-year interval, the system is sufficiently noisy that whatever changes are taking place cannot be distinguished against the large interannual variability. Although it is possible that trends become apparent through the much longer multi-decadal span considered in the ventilation discussion, the extremely thin and poorly distributed in situ observations before the 1990s render unattainable the useful estimation of any global average (see the sampling discussion in Wunsch et al., 2007).

7 Discussion

Global solutions such as the ones used here describe a very large range of phenomena calling out for details and explanation (keeping in mind the distortions implied by two-dimensional projections, and the need to avoid interpreting the resulting Eulerian mean velocities as particle trajectories). We have only touched on some of the more conspicuous fluctuations seen primarily in the tropics and the perhaps more surprising variability in the deep Southern Ocean, but without pursuing the details of either. The great bulk of the variability variance in the global MOC and its corresponding enthalpy transports over the 15-year interval, lies in the annual cycle, and which at lowest order is consistent with the simplest expectations of linear Rossby wave dynamics (cf. Gill and Niiler, 1973). This same theory strongly supports the inference that, absent a finite amplitude ocean disturbance, multiple decades are required to detect deep ocean changes.

No evidence has been found that the ocean has been or is undergoing any change sufficient to require moving beyond perturbation theory. The changes seen in the ECCO-GODAE estimate are small disturbances to the fully-established general circulation although the annual cycle forcing is always very large. Linear theory (Veronis and Stommel, 1955; Pedlosky, 2003; see Gill, 1984 for a full account) shows that in the perturbation regime, large decadal changes in baroclinic structures are not expected outside of the tropics. No sign exists of any significant trends or unusual behavior in the MOC over the last 15 years. What the future will bring is another question, but the implications of perturbation theory, the very large eddy noise present in the real system, and the enormous potential energy of the existing stratification all militate against the expectation of seeing major shifts on time scales shorter than many decades. Suggestions that the ocean circulation is or could be changing into radically different states need to address the energy sources required to make a qualitative change in the potential energy reservoirs.

What of the future? The dominant variability as seen here is (1) annual and semi-annual, (2) a few weak trends with complex spatial patterns, and (3) a long memory in the sub-surface ocean. Anomalies propagating at depth in northern latitudes will require some decades to adjust the system and their presence is likely to produce some degree of local high latitude predictability.[3] The general linear theory of the prediction of stationary time series (Yaglom, 1962) shows that more spectral structure produces longer prediction horizons. Thus a narrow-band annual cycle can be predicted many years into the future, as can a general red noise process. The stability of the annual cycle components, apart from the reaction of some singular vectors to the large ENSO of 1997-1998, remains in keeping with the notion that only subtle changes have taken place in the ocean circulation since 1992.

Acknowledgements. Supported in part by the National Ocean Partnership Program (NOPP) with additional funding from the National Aeronautics and Space Administration. Computations were carried out at the National Center for Atmospheric Research (NSF funded), the Geophysical Fluid Dynamics Laboratory (NOAA) and elsewhere. Comments by M. Mazloff, and A. Naveira Garabato were helpful.

[3] Hawkins and Sutton (2007) discuss the *much longer* time-scale variability of the global MOC within a coupled atmosphere-ocean model, but one unconstrained by any observations.

References

Bindoff, N. L. and 12 others, 2007: Observations: oceanic climate change and sea level. In *Climate Change 2007: The Physical Science Basis. Contribution of Working Group I to the Fourth Assessment Report of the IPCC.* S. Solomon et al., Eds. 386-432. Cambridge Un. Press. Cambridge

Björck, A., 1996: *Numerical Methods for Least Squares Problems*. SIAM, Philadelphia, 408pp.

Boccaletti, G., R. Ferrari, A. Adcroft, J. Marshall, 2005: The vertical structure of ocean heat transport. *Geophys. Res. Letts.*, 32, L10603.

Cessi, P., K. Bryan and R. Zhang, 2004: Global seiching of thermocline waters between the Atlantic and the Indian-Pacific Ocean basins. *Geophys. Res. Letts.*, 31, doi:10.1029/2003GL019091.

Cunningham, S. and M. Pavic, 2007: Surface geostrophic currents across the Antarctic Circumpolar Current in Drake Passage from 1992 to 2004. *Prog. Oceanog.*, 73, 296-310.

Ferrari, R. and C. Wunsch, 2009: Ocean circulation kinetic energy—Reservoirs, sources and sinks. *Ann Rev. Fluid Mech.,* to appear.

Ganachaud, A. and C. Wunsch, 2002: Large-scale ocean heat and freshwater transports during the World Ocean Circulation Experiment. *J. Clim.*, 16, 696-705.

Gill, A. E. and P. P. Niiler, 1973: The theory of the seasonal variability in the ocean. *Deep-Sea Res.*, 20, 141-177.

Gill, A. E., 1982: *Atmosphere-Ocean Dynamics.* Academic Press, New York, 662 pp.

Hawkins, E. and R. Sutton, 2007: Variability of the Atlantic thermohaline circulation described by three-dimensional empirical orthogonal functions. *Clim. Dyn.,* 29, 745-762.

Hurrell, J. W. and 18 others, 2006: Atlantic climate variability and predictability: CLIVAR perspective. *J. Clim.* , 19, 5100-5121.

Ivchenko, V. O., A. M. Treguier, S. E. Best, 1997: A kinetic energy budget and internal instabilities in the Fine Resolution Antarctic Model. *J. Phys. Oc.*, 27, 5-22.

Johnson, G. C., M. J. McPhaden, and E. Firing, 2001: Equatorial Pacific Ocean horizontal, velocity, divergence, and upwelling. *J. Phys. Oc.*, 32, 839-849.

Jolliffe, I. T., 2002: *Principal Component Analysis*, 2nd Ed. Springer-Verlag, New York, 487271 pp.

Kalnay, E. and 21 others, 1996: The NCEP/NCAR 40-year reanalysis project. *Bull. Am. Met. Soc.*, 77, 437-471.

Keenlyside, N. and R. Kleeman, 2002: Annual cycle of equatorial zonal currents in the Pacific. *J. Geophys. Res.*, 107, C8, DOI 10.1029/200JC00711.

Lumpkin, R. and K. Speer, 2007: Global meridional overturning. *J. Phys. Oc.*, 37, 2550-2562.

Meehl, G. A., 1991:A reexamination of the mechanism of the semiannual oscillation in the southern hemisphere. *J. Clim.*, 4, 911-926.

Olbers, D. and K. Lettmann, 2007: Barotropic and baroclinic processes in the transport variability of the Antarctic Circumpolar Current. *Ocean Dyn.*, 57, 559-578.

Pedlosky, J. , 2003: *Waves in the Ocean and Atmosphere: Introduction to Wave Dynamics.* Springer, Berlin, 250pp.

Rabe, B., F. A. Schott and A. Köhl, 2008: Mean circulation and variability of the tropical Atlantic during 1952-2001 in the GECCO assimilation fields. *J. Phys. Oc.*, 38, 177-192.

Scott, J. R. and J. Marotzke, 2002: The location of diapycnal mixing and the meridional overturning circulation. *J. Phys. Oc.*, 32, 3578-3595.

Sturges, W., B. G. Hong, A. J. Clarke, 1998: Decadal wind forcing of the North Atlantic subtropical gyre. *J. Phys. Oc.*, 28, 659-668.

Talley, L. D., 2003: Shallow, intermediate, and deep overturning components of the global heat budget. *J. Phys. Oc.*, 33, 530-560.

Thompson, D. W. J. and J. M. Wallace, 2000: Annular modes in the extratropical circulation. Part I: month-to-month variability. *J. Clim.*, 13, 1000-1016.

D. W. J. Thompson, J. M. Wallace, G. C. Hegerl, 2000: Annular modes in the extratropical circulation. Part II: trends. *J. Clim.*, 13, 1018-1036.

Trenberth, K. E., W. G. Large, and J. G. Olson, 1989: The mean annual cycle in global ocean wind stress.*J. Phys. Oc.*, 20, 1742-1760.

Veronis, G. and H. Stommel, 1956: The action of variable wind stresses on a stratified ocean. *J. Mar. Res.*, 15, 43-75.

von Storch, H. and F. W. Zwiers, 1999: *Statistical Analysis in Climate Research.* Cambridge Un. Press, 484pp.

Webb, D. J. and B. A. de Cuevas, 2007: On the fast response of the Southern Ocean to changes in the zonal wind. *Ocean Sci.*, 3, 417-427

Wunsch, C. and P. Heimbach, 2008: How long to ocean tracer and proxy equilibrium? *Quat. Sci. Rev.*, in press.

Wunsch, C., 2005: The total meridional heat flux and its oceanic and atmospheric partition. *J. Clim.*, 18, 4374-4380.

Wunsch, C. 2008: Mass and volume transport variability in an eddy-filled ocean. *Nature Geosci.,* doi:10.1038/ngeo126.

Yaglom, A. M, 1962: *An Introduction to the Theory of Stationary Random Functions.* 235

pp. R. A. Silverman, translator, Prentice-Hall, Englewood Cliffs, NJ.

8 Appendix 1. EOFs and the Singular Value Decomposition

At fixed time $t = t_p$, V' is a matrix with rows defining depths, and columns the latitude. For each such time, make a column vector of the matrix,

$$\mathbf{a}_p\left(t_p\right) = \operatorname{vec}\left(V'\left(\phi_j, z_k, t_p\right)\right),$$

and a new matrix $\mathbf{A}$ is defined by these columns:

$$\mathbf{A} = \left\{\mathbf{a}_p\right\}.$$

By the Eckart-Young-Mirsky Theorem (e.g. Björck, 1996, P.12)

$$\mathbf{A} \approx \sum_{j=1}^{K} \lambda_j \mathbf{u}_j \mathbf{v}_j^T \qquad (1)$$ {svd1}

gives the most efficient possible representation of $\mathbf{A}$ for any set of K orthonormal column vectors $\mathbf{u}_j$, $\mathbf{v}_j$ if they are chosen as the singular vectors, and λ_j are the singular values. (The $\mathbf{u}_j$ are commonly called the empirical orthogonal functions, EOFs, a terminology we will use interchangeably, but the singular value decomposition form is more physically immediate.) The singular vectors $\mathbf{v}_j$ should not be confused with the meridional velocity component v. If $K = \min\left(M, N, \operatorname{rank}\left(\mathbf{A}\right)\right)$ then Eq. (1) becomes an equality.

As always, the hope is that the required $K = K_{eff}$, the "effective" rank, is small. A simple measure of effectiveness is that $\sum_{j=1}^{K_{eff}} \lambda_j^2 / \sum_{j=1}^{K} \lambda_j^2$ represents the fraction of the variance of components of $\mathbf{A}$ described by Eq. (1) measured as the square of the matrix Frobenius norm of the difference of $\mathbf{A}$ from its singular value decomposition truncated at $j = K$. As has been widely recognized, in part because of the space/time orthogonality requirement, the singular vectors need not have a simple physical interpretation (although they may), but are best regarded as an empirical, maximally efficient, description of covariability in the fields.

The references (e.g., Jolliffe, 2002; von Storch and Zwiers, 1999) discuss the statistical reliability of these calculations. It is well known that the singular values are more robustly determined than are the corresponding singular vectors. Jolliffe (2002, P. 42+ provides approximate confidence intervals for both, and von Storch and Zwiers (1999, P. 303) discuss a useful simplification. In the present case, the λ_j have negligible uncertainty, but the EOF (singular vector) structures are unstable when the singular values are close to others. Thus the discussion here is generally limited to the low, terms corresponding to widely separated λ_i.

9 Appendix 2. Higher Order EOFs

As discussed in Appendix 1, singular vectors corresponding to clustered λ_i will be unstable in their spatial structure. For that reason, only the lowest and most robust ones are displayed in the text. But because there is important information, particularly in the temporal variations, about their physics, we here display a few of the higher order EOFs of volume and temperature transport, as well as for temperature itself (Figs.20-25).

Figure Captions

1. Time for a disturbance traveling with the group velocity of a Rossby wave of wavelength $L = 5000$km to cross a basin of width L (shorter waves can take much longer). A fixed Rossby radius of 30km was used, and only β permitted to change with latitude. (See Veronis and Stommel, 1956, although here a continuously layered ocean was used.) At high latitudes, decades are required to begin the adjustment process even accounting for basin narrowing and the large changes in deformation radius.

2. Mean (1992-2006) of the meridional volume flux in Sverdrups (Sv-10^6m^3/s) from ECCO-GODAE v3.22. Note the complex equatorial structure in the Atlantic and Pacific. Contour interval is 1Sv. In the Southern Ocean, interpretation of zonally integrated Eulerian means requires particular care owing to the complex topography and relatively important eddy transport field.

3. Same as Fig. 2 except showing the upper 300m. Notice in particular the complex structure at and near the equator in all oceans.

4. Maximum meridional volume transport values (Sv), irrespective of sign for the time-mean in each basin (solid curve, left axis) and the depth (dashed curve, right axis) to which one must integrate to achieve the maximum.

5. $\bar{W}(\phi, z,)$, the zonally summed time-mean vertical velocity, w, in 0.01 Sverdrups at intervals of 2.5×10^{-3} Sv. Patterns are complex and difficult to summarize. In the North Atlantic, the strong downwelling near 65°N is close to but not the same as the region of convection (see Scott and Marotzke, 2002). A conspicuous Deacon Cell appears in the Southern Ocean, but the reader is reminded of the caveat not to interpret two dimensional time-average projections of Eulerian mean velocities as corresponding to particle velocities.

6. Upper 1000m of the time average temperature transport.

7. Temporal variance (from monthly means) of $V(\phi, z, t)$ in the v3.22 solution. Contour interval is 3Sv^2. As the simple theory in Fig. 1 implies, the system is dominated by fluctuations at low latitudes over decadal time scales, with little relative variability expected or seen at high latititudes. Southern Ocean excess variance at depth is likely associated with the special dynamics of the topographic interactions there at those depths driven by a forceful barotropic field. Total variance is $(0.83\text{Sv})^2$ with the great mass of the Pacific Ocean dominating.

8. First global volume transport variability EOF (singular vector), $\mathbf{u}_1$, with about 43% of the total variance displayed in each ocean basin (a-d). This mode evidently represents the predominant and strong annual cycle in volume transport, and like most of the variability seen is largely tropical and dominated by the Pacific and Indian Oceans. Little North Atlantic response is visible (only contours with magntiude greather than or equal to 0.01 are shown). Consistent with linear theory, the Pacific response has a somewhat barotropic nature below the very surface layers. Panel (e) displays $\mathbf{v}_1(t)$ and its power spectral density estimate, with the first two years omitted from the analysis here and in the other plots.. A hint of an ENSO response is visible (vertical dashed line in the plot of $\mathbf{v}_1$) is the 1997-1998 transition time. Vertical dashed lines on the spectral density of $\mathbf{v}_1(t)$ (f) denote the annual and semiannual periods.

9. Second EOF with about 8% of the temporal variance, is also dominantly annual in character but with a visible ENSO disturbance in the $\mathbf{v}_2(t)$ plot. Both the amplitude and phase recover quickly.

10. First heat content (temperature) EOF with 58% of the temporal variance. A general warming above 1000m is seen except in the poleward latitudes of the Southern Ocean, and in most deeper parts of all basins.

11. Second temperature EOF with about 19% of the variance and which is a surface annual cycle showing a 180° phase change between the hemispheres. Note that only the top 300m are displayed as the amplitudes are very small below that—consistent with the general expectation of the penetration of the annual thermal signal.

12. Estimate, with one standard deviation error bars, of the ocean (dashed) and atmospheric (dash-dot) meridional enthalpy fluxes (adapted from Wunsch, 2005, primarily from results of Ganachaud and Wunsch, 2002). The major inference is that poleward of about 50° in both hemispheres, the mean oceanic component is very small, and hence little variability in its values would be expected or is seen. Although the hydrographic sections used to make the estimates are also part of the ECCO-GODAE data sets, the model used by Ganachaud and Wunsch (2002) is a very different one from the GCM. Atmospheric values were computed as a residual of the ocean circulation transports subtracted from earth radiation budget values. That the changing MOC at high latitudes is a major cause of climate change, other than regionally, is very implausible given the minute contribution the ocean makes to the meridional heat transport there.

13. Total heat transport in each basin and the global total from ECCO-GODAE v3.22. The total (lowest panel) does not show as great an anti-symmetry as seen in the ocean estimate in

Fig. 12, but the estimates are consistent within the error bars of that figure alone, without consideration of the uncertainty of the model itself.

14. First EOF (singular vector $\mathbf{u}_1$) of the meridional enthalpy (heat) transport. Because of the strong surface confinement, only the top 300m are shown. The first EOF corresponds to about 60% of the heat transport variance and is an essentially annual mode confined to the tropics.

15. Second EOF of the meridional heat transport fluctuations, with about 9% of the variance. The major features remain the annual cycle and the tropical confinement, but with a visible ENSO signal now present.

16. First EOF, with about 39% of the variability, in τ_x. It is essentially the annual variability and dominated by the low latitude Southern Ocean, with major contributions in the tropics (with the exception of the Atlantic). The Pacific and Indian Oceans have a remarkable near-perfect anti-symmetry about the equator (vanishing there).

17. Second τ_x EOF with about 26% of the variance. This mode is broadband, with an excess of semi-annual variability and is dominated by Southern Ocean winds at the AAC latitudes. (Note change of scale in the Southern Ocean.)

18. First EOF of the enthalpy (heat) flux from the atmosphere. This mode contains a remarkable 96% of the total variability variance and is nearly anti-symmetric about the equator.

19. Second heat flux from the atmosphere EOF, but with less than about 1.5% of the variance.

20. Third meridional volume transport EOF with about 7% of the variance is still tropically dominated, but exhibits an early trend disappearing later in the calculation.

21. Fourth meridional transport EOF, with about 4.5% of the variance, now dominantly semi-annual in character and again primarily tropical but with a visible signature in the deep Southern Ocean.

22. Fifth volume transport variability EOF with 4% of the variance. The common spatial structure of the trend and the 6-month peak variance might be coincidence.

23. Third temperature variability EOF with about 6% of the variance. Note the differing depth ranges.

24.Third EOF of the enthalpy transport, with about 6% of the variance and a dominantly 6 month time-scale. An ENSO signal is again present.

25. Fourth enthalpy transport EOF with about 4% of the variability variance and again a dominantly 6 month time scale. {1}

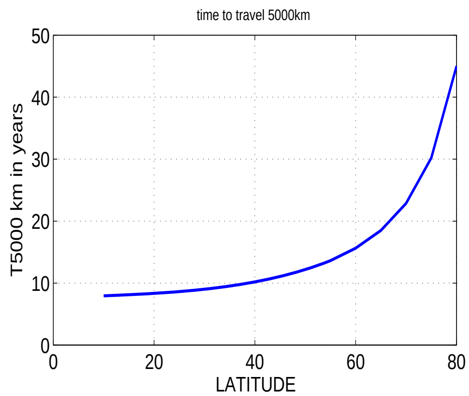

Figure 1: Time for a disturbance traveling with the group velocity of a Rossby wave of wavelength $L = 5000$km to cross a basin of width L (shorter waves can take much longer). A fixed Rossby radius of 30km was used, and only β permitted to change with latitude. (See Veronis and Stommel, 1956, although here a continuously layered ocean was used.) At high latitudes, decades are required to begin the adjustment process even accounting for basin narrowing and the large changes in deformation radius.

{rossbytimes.e

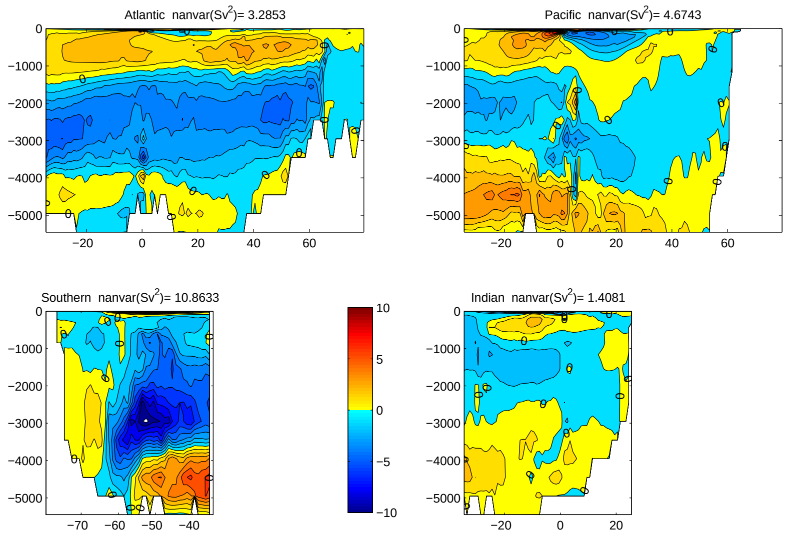

Figure 2: Mean (1992-2006) of the meridional volume flux in Sverdrups (Sv-10^6m^3/s) from ECCO-GODAE v3.22. Note the complex equatorial structure in the Atlantic and Pacific. Contour interval is 1Sv. In the Southern Ocean, interpretation of zonally integrated Eulerian means requires particular care owing to the complex topography and relatively important eddy transport field. {mean_merid.ep

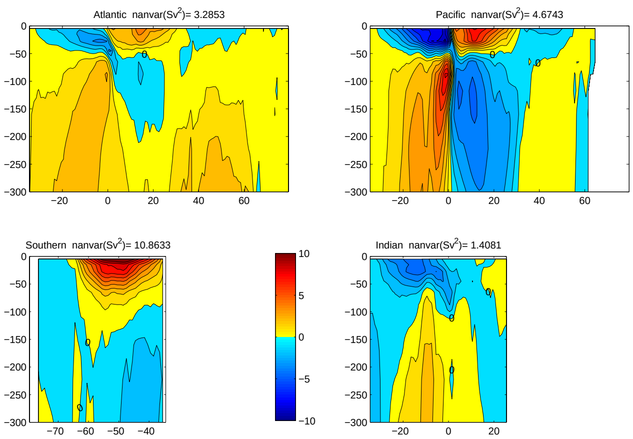

Figure 3: Same as Fig. 2 except showing the upper 300m. Notice in particular the complex structure at and near the equator in all oceans.

{mean_merid_up

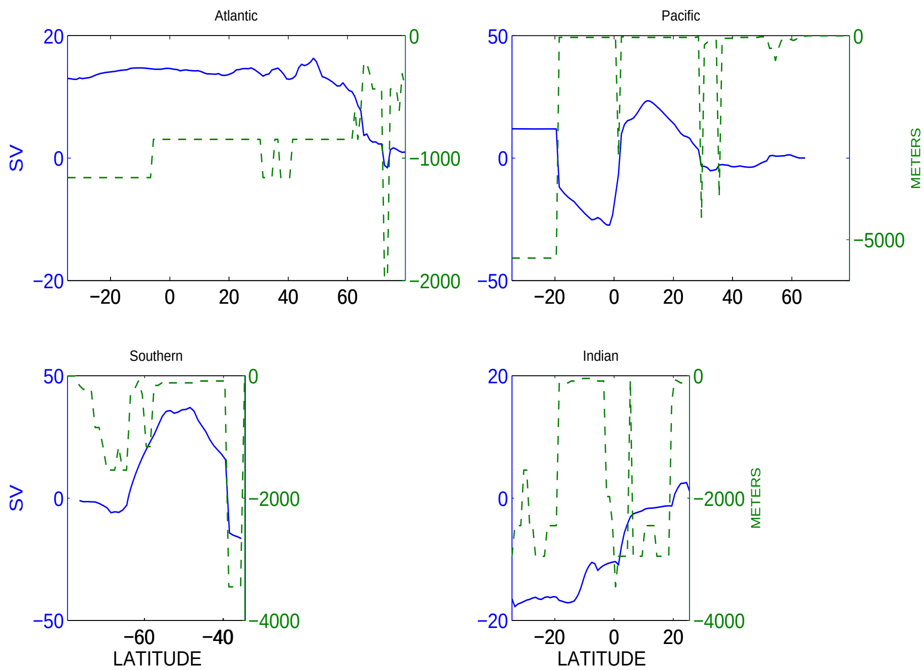

Figure 4: Maximum meridional volume transport values (Sv), irrespective of sign for the time-mean in each basin (solid curve, left axis) and the depth (dashed curve, right axis) to which one must integrate to achieve the maximum.

{max_trans.eps

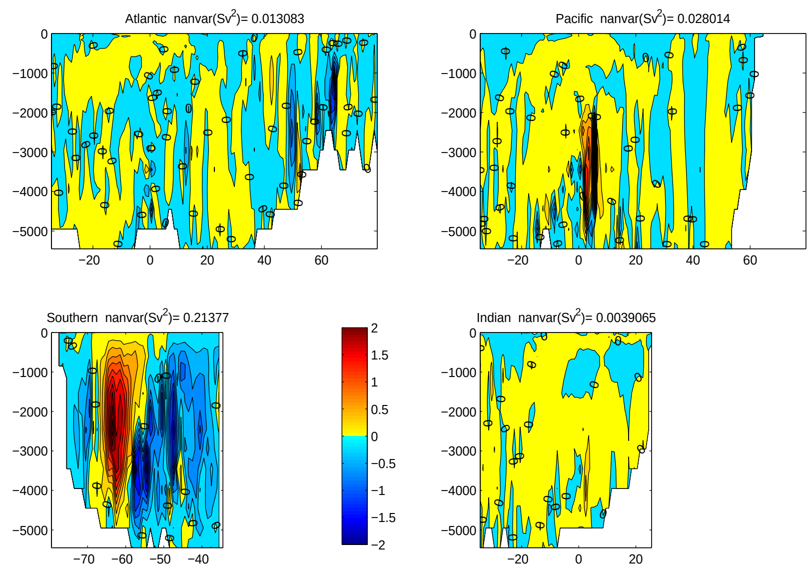

Figure 5: $\bar{W}(\phi, z,)$, the zonally summed time-mean vertical velocity, w, in 0.01 Sverdrups at intervals of 2.5×10^{-3} Sv. Patterns are complex and difficult to summarize. In the North Atlantic, the strong downwelling near 65°N is close to but not the same as the region of convection (see Scott and Marotzke, 2002). A conspicuous Deacon Cell appears in the Southern Ocean, but the reader is reminded of the caveat not to interpret two dimensional time-average projections of Eulerian mean velocities as corresponding to particle velocities.

{global_w.eps}

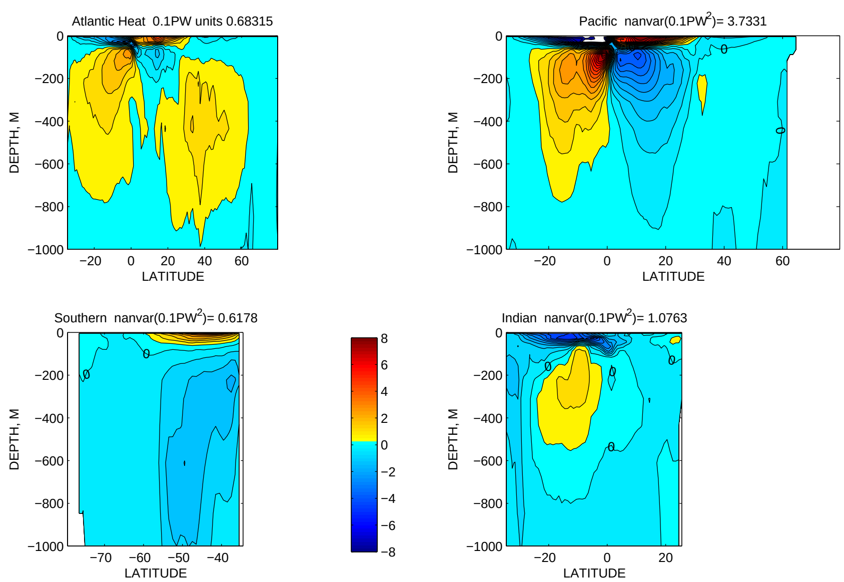

Figure 6: Upper 1000m of the time average temperature transport. {global_heat_t

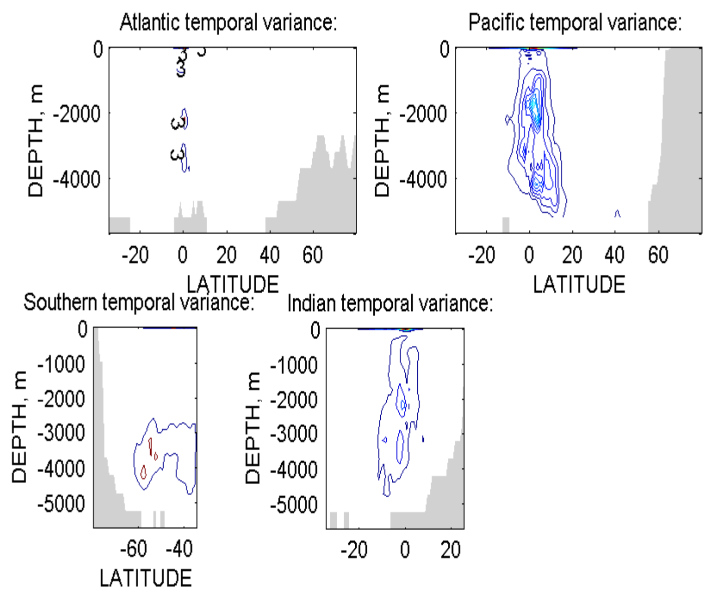

Figure 7: Temporal variance (from monthly means) of $V(\phi, z, t)$ in the v3.22 solution. Contour interval is $3\mathrm{Sv}^2$. As the simple theory in Fig. 1 implies, the system is dominated by fluctuations at low latitudes over decadal time scales, with little relative variability expected or seen at high latititudes. Southern Ocean excess variance at depth is likely associated with the special dynamics of the topographic interactions there at those depths driven by a forceful barotropic field. Total variance is $(0.83\mathrm{Sv})^2$ with the great mass of the Pacific Ocean dominating.

{temporalvaria

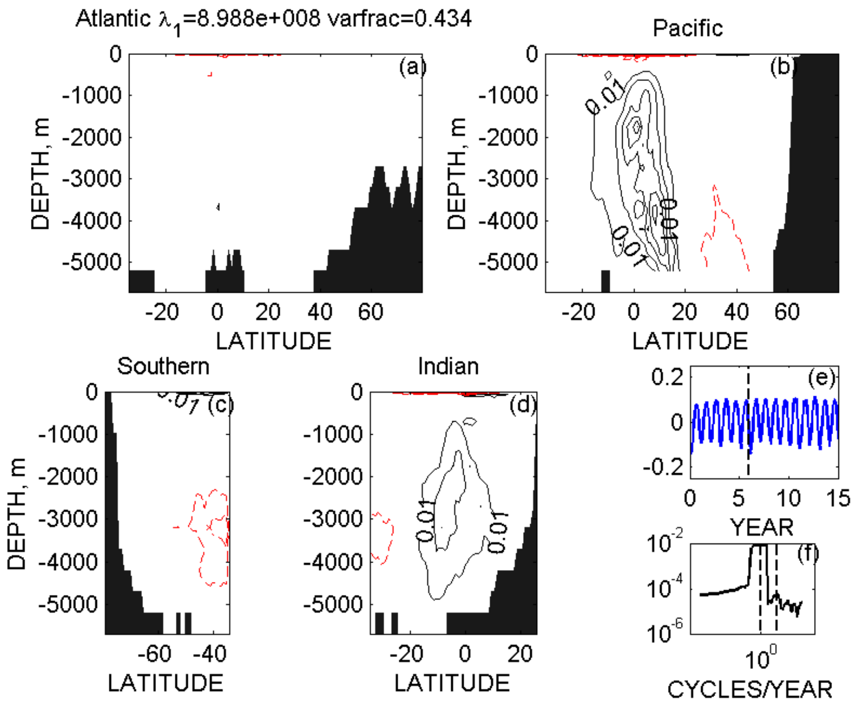

Figure 8: First global volume transport variability EOF (singular vector), $\mathbf{u}_1$, with about 43% of the total variance displayed in each ocean basin (a-d). This mode evidently represents the predominant and strong annual cycle in volume transport, and like most of the variability seen is largely tropical and dominated by the Pacific and Indian Oceans. Little North Atlantic response is visible (only contours with magntiude greather than or equal to 0.01 are shown). Consistent with linear theory, the Pacific response has a somewhat barotropic nature below the very surface layers. Panel (e) displays $\mathbf{v}_1(t)$ and its power spectral density estimate, with the first two years omitted from the analysis here and in the other plots.. A hint of an ENSO response is visible (vertical dashed line in the plot of $\mathbf{v}_1$) is the 1997-1998 transition time. Vertical dashed lines on the spectral density of $\mathbf{v}_1(t)$ (f) denote the annual and semiannual periods.

{global_sv1.ep

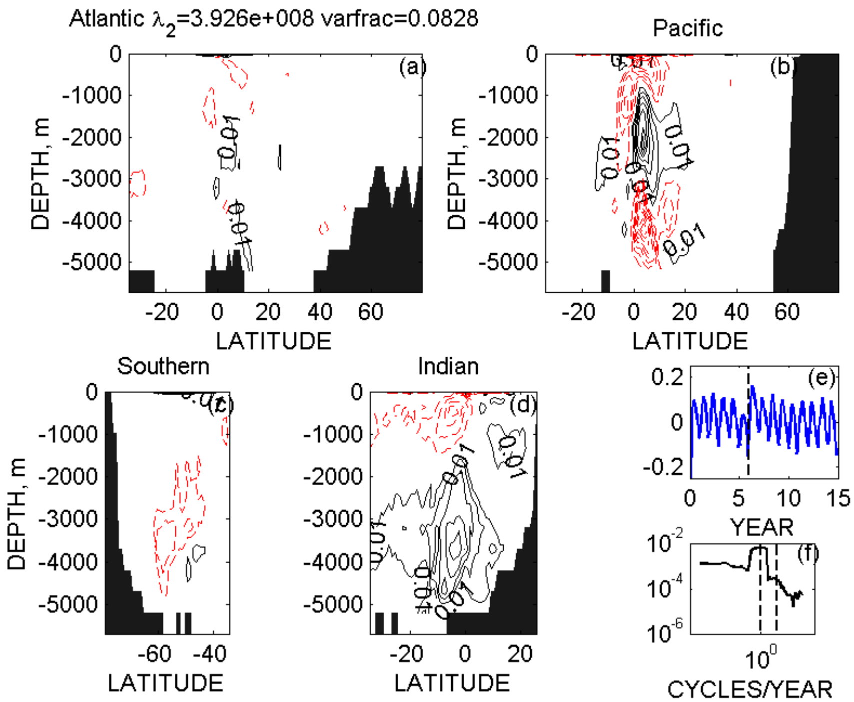

Figure 9: Second EOF with about 8% of the temporal variance, is also dominantly annual in character but with a visible ENSO disturbance in the $\mathbf{v}_2(t)$ plot. Both the amplitude and phase recover quickly. {global_sv2.ep

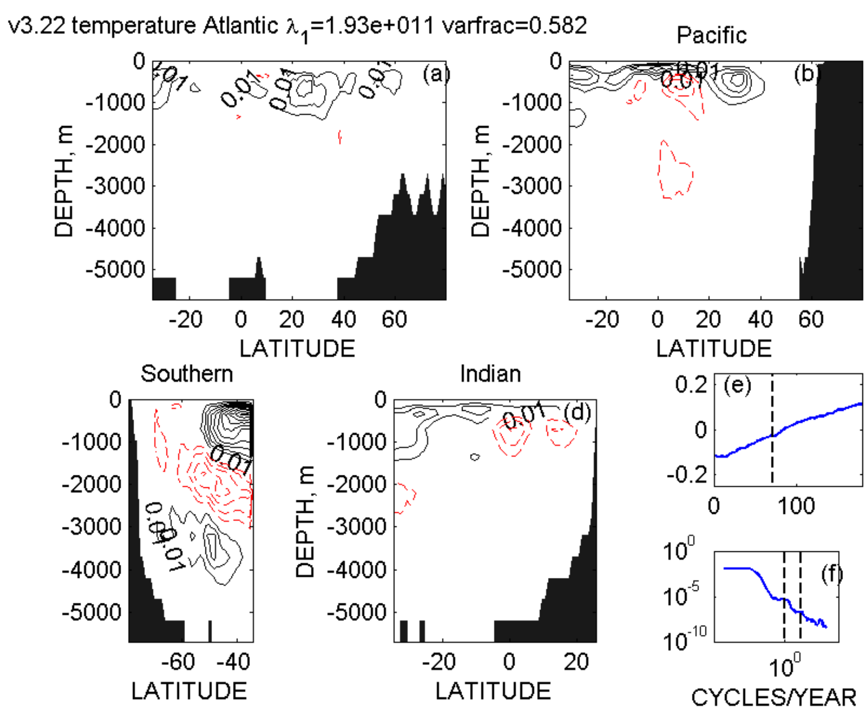

Figure 10: First heat content (temperature) EOF with 58% of the temporal variance. A general warming above 1000m is seen except in the poleward latitudes of the Southern Ocean, and in most deeper parts of all basins.

{temper_sv1.ep

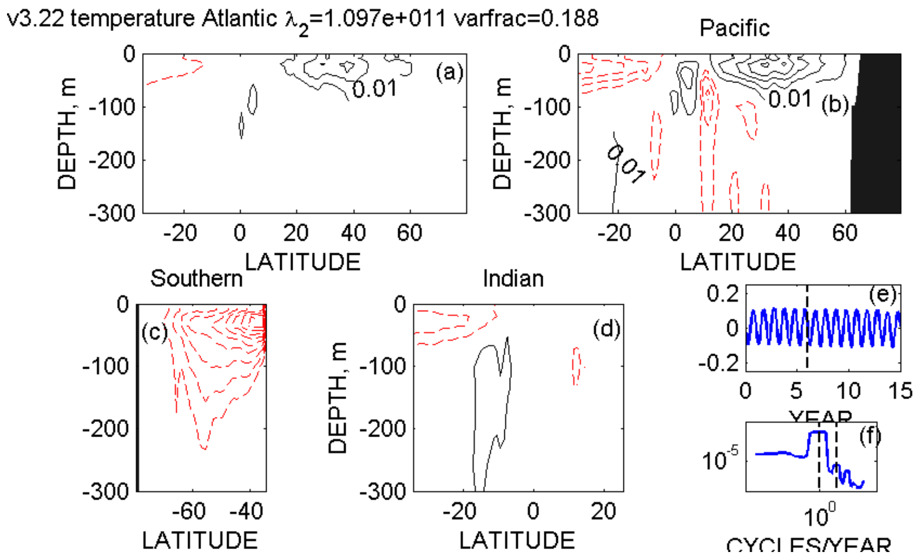

Figure 11: Second temperature EOF with about 19% of the variance and which is a surface annual cycle showing a 180° phase change between the hemispheres. Note that only the top 300m are displayed as the amplitudes are very small below that—consistent with the general expectation of the penetration of the annual thermal signal.

{temper_sv2.ep

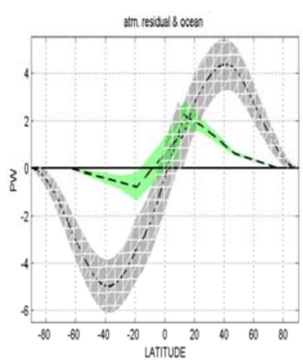

Figure 12: Estimate, with one standard deviation error bars, of the ocean (dashed) and atmospheric (dash-dot) meridional enthalpy fluxes (adapted from Wunsch, 2005, primarily from results of Ganachaud and Wunsch, 2002). The major inference is that poleward of about 50° in both hemispheres, the mean oceanic component is very small, and hence little variability in its values would be expected or is seen. Although the hydrographic sections used to make the estimates are also part of the ECCO-GODAE data sets, the model used by Ganachaud and Wunsch (2002) is a very different one from the GCM. Atmospheric values were computed as a residual of the ocean circulation transports subtracted from earth radiation budget values. That the changing MOC at high latitudes is a major cause of climate change, other than regionally, is very implausible given the minute contribution the ocean makes to the meridional heat transport there.

{atmoceanalone

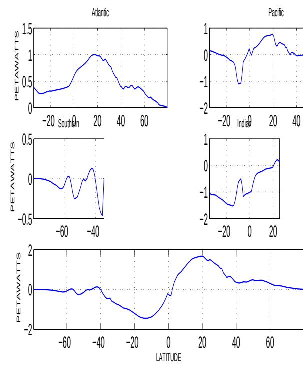

Figure 13: Total heat transport in each basin and the global total from ECCO-GODAE v3.22. The total (lowest panel) does not show as great an anti-symmetry as seen in the ocean estimate in Fig. 12, but the estimates are consistent within the error bars of that figure alone, without consideration of the uncertainty of the model itself. {total_heat_tr

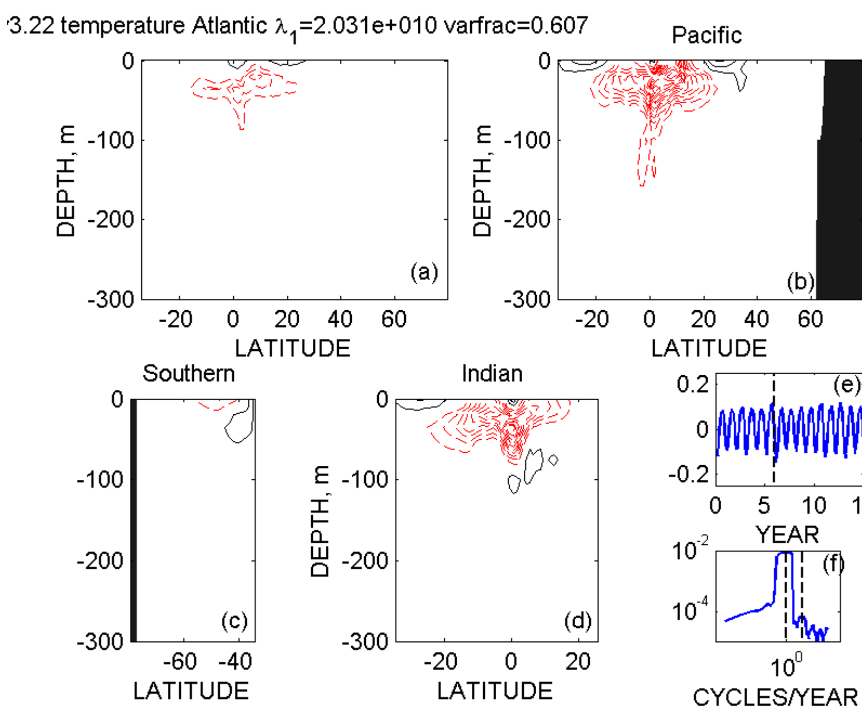

Figure 14: First EOF (singular vector $\mathbf{u}_1$) of the meridional enthalpy (heat) transport. Because of the strong surface confinement, only the top 300m are shown. The first EOF corresponds to about 60% of the heat transport variance and is an essentially annual mode confined to the tropics. {global_heat_s

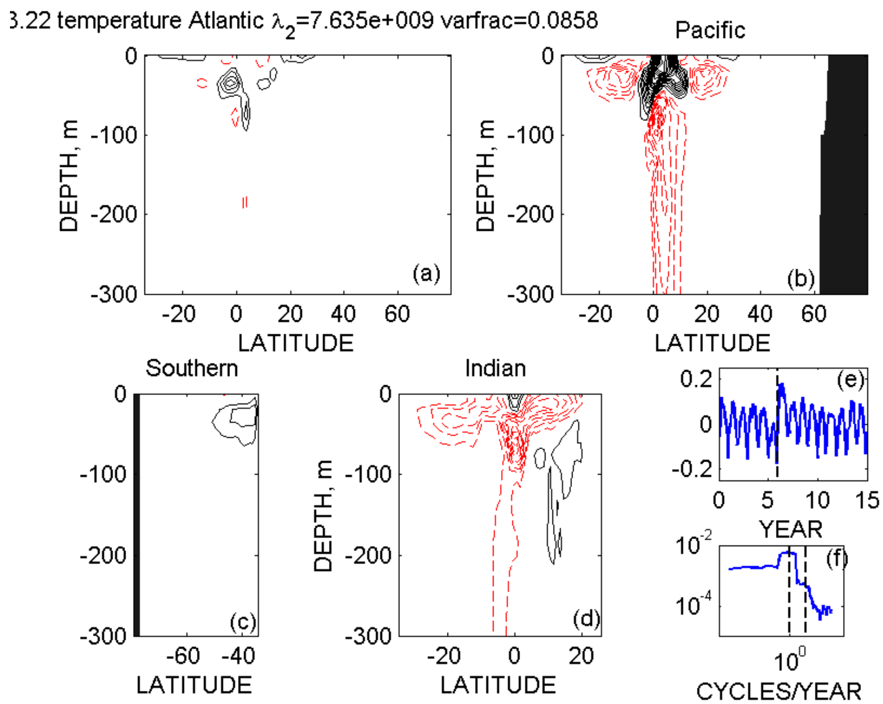

Figure 15: Second EOF of the meridional heat transport fluctuations, with about 9% of the variance. The major features remain the annual cycle and the tropical confinement, but with a visible ENSO signal now present.

{global_heat_s

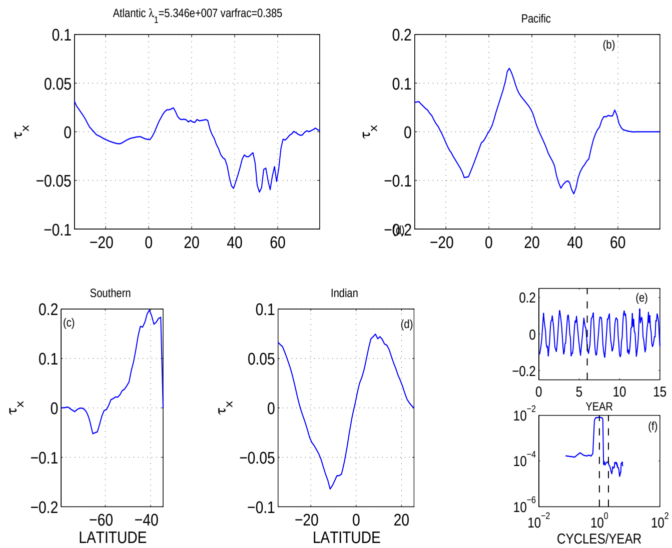

Figure 16: First EOF, with about 39% of the variability, in τ_x. It is essentially the annual variability and dominated by the low latitude Southern Ocean, with major contributions in the tropics (with the exception of the Atlantic). The Pacific and Indian Oceans have a remarkable near-perfect anti-symmetry about the equator (vanishing there).

{taux_sv1.eps}

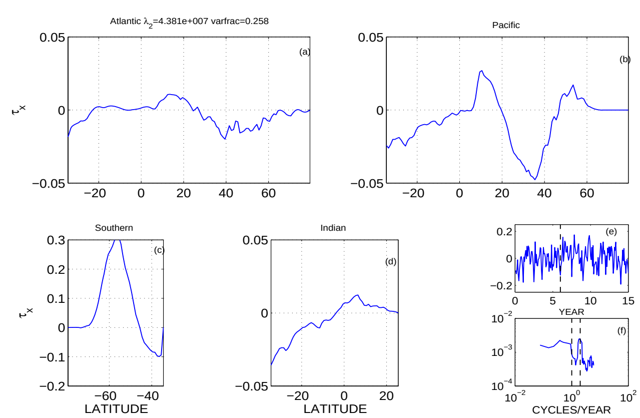

Figure 17: Second τ_x EOF with about 26% of the variance. This mode is broadband, with an excess of semi-annual variability and is dominated by Southern Ocean winds at the AAC latitudes. (Note change of scale in the Southern Ocean.)

{taux_sv2.eps}

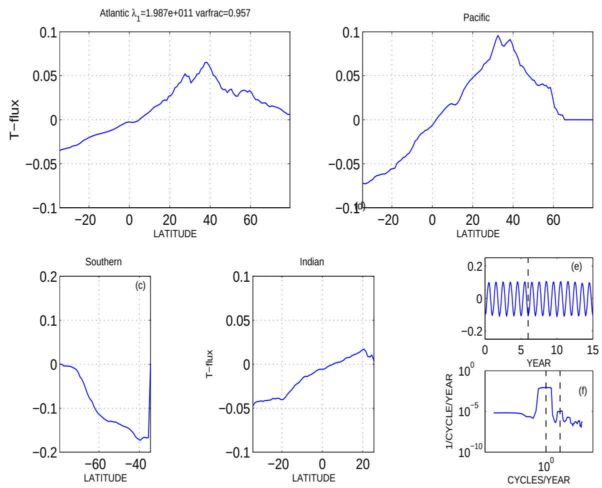

Figure 18: First EOF of the enthalpy (heat) flux from the atmosphere. This mode contains a remarkable 96% of the total variability variance and is nearly anti-symmetric about the equator. {heat_sv1.eps}

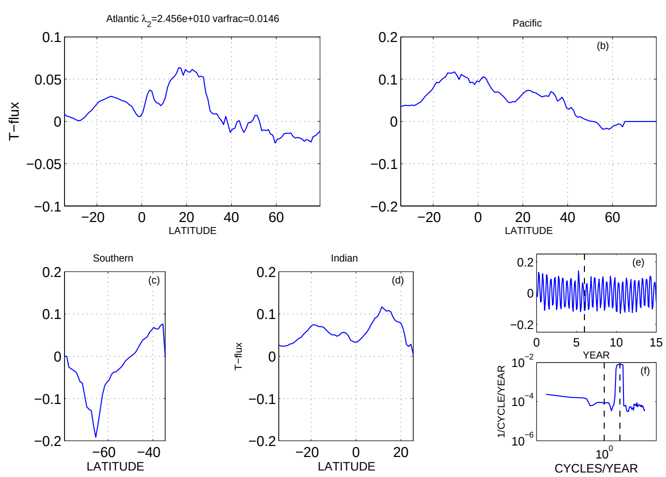

Figure 19: Second heat flux from the atmosphere EOF, but with less than about 1.5% of the variance. {heat_sv2.eps}

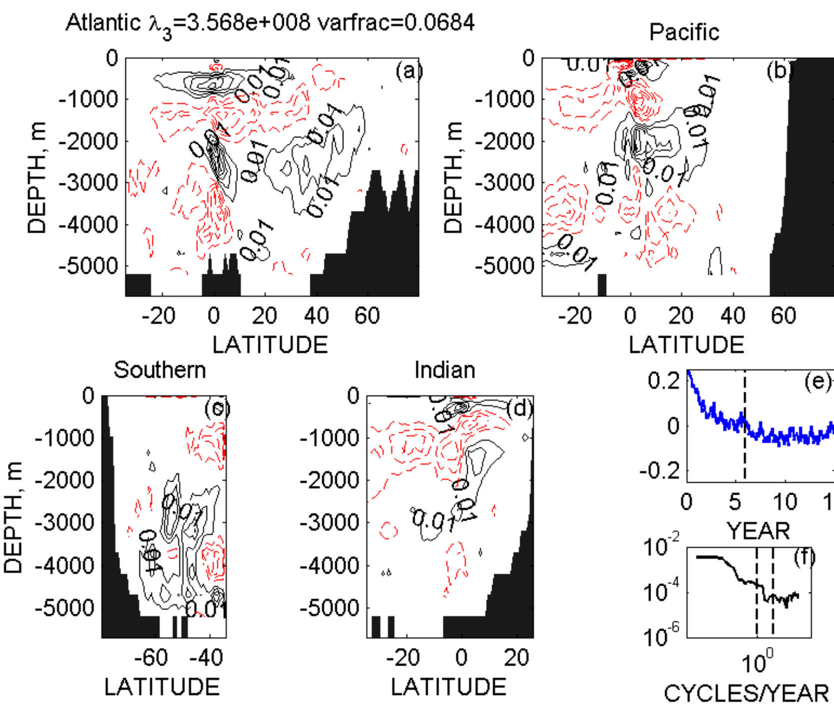

Figure 20: Third meridional volume transport EOF with about 7% of the variance is still tropically dominated, but exhibits an early trend disappearing later in the calculation.

{global_sv3.ep

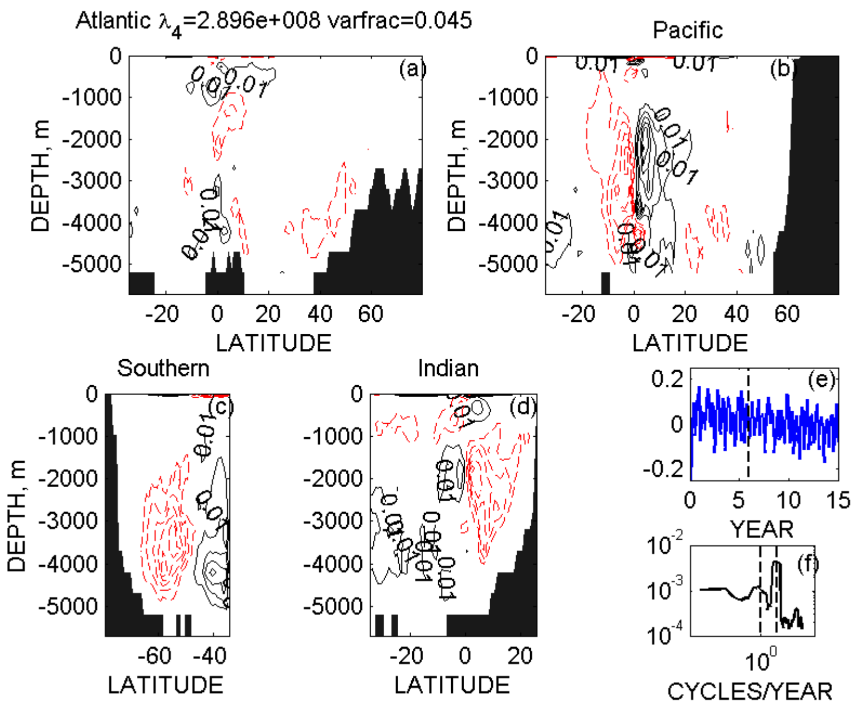

Figure 21: Fourth meridional transport EOF, with about 4.5% of the variance, now dominantly semi-annual in character and again primarily tropical but with a visible signature in the deep Southern Ocean.

{global_sv4.ep

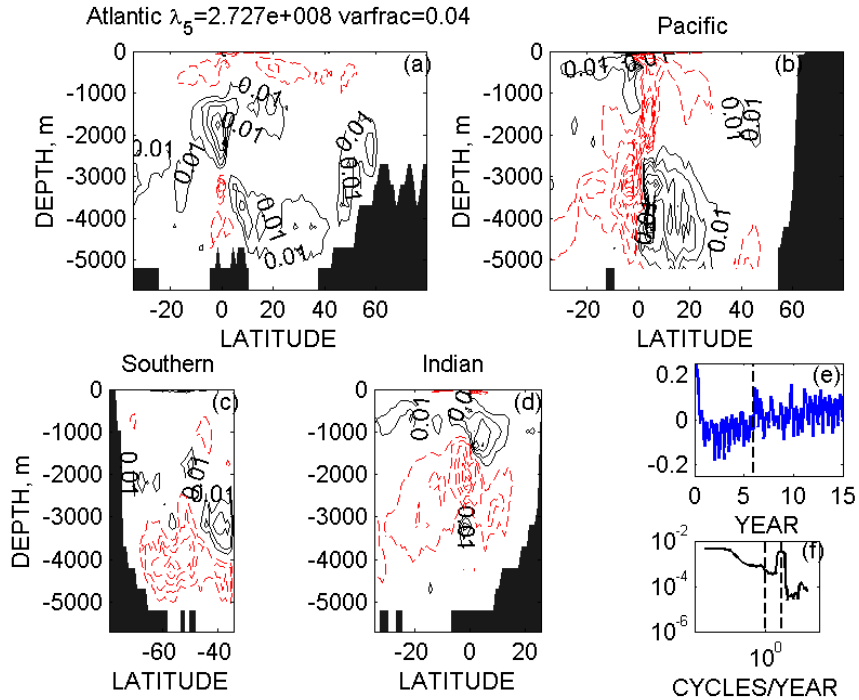

Figure 22: Fifth volume transport variability EOF with 4% of the variance. The common spatial structure of the trend and the 6-month peak variance might be coincidence.

{global_sv5.ep

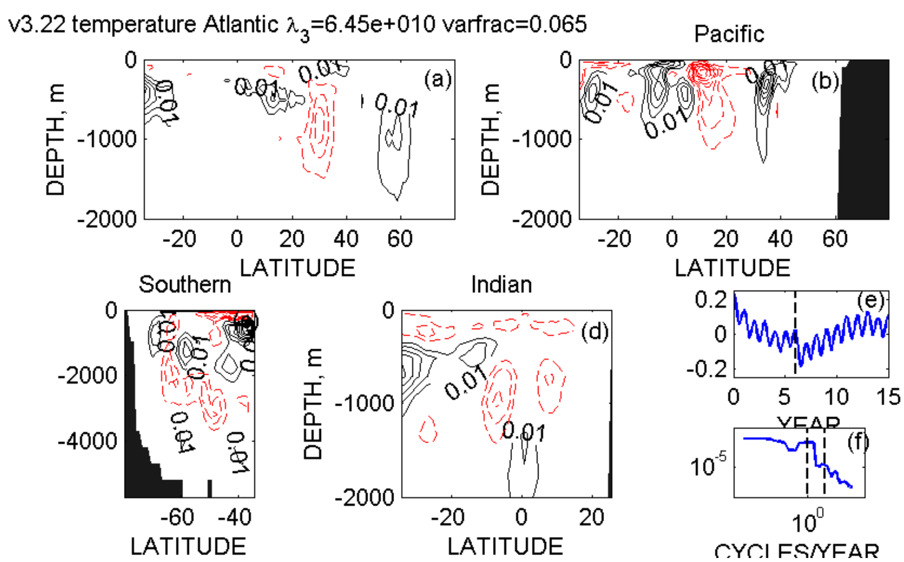

Figure 23: Third temperature variability EOF with about 6% of the variance. Note the differing depth ranges.

{temper_sv3.ep

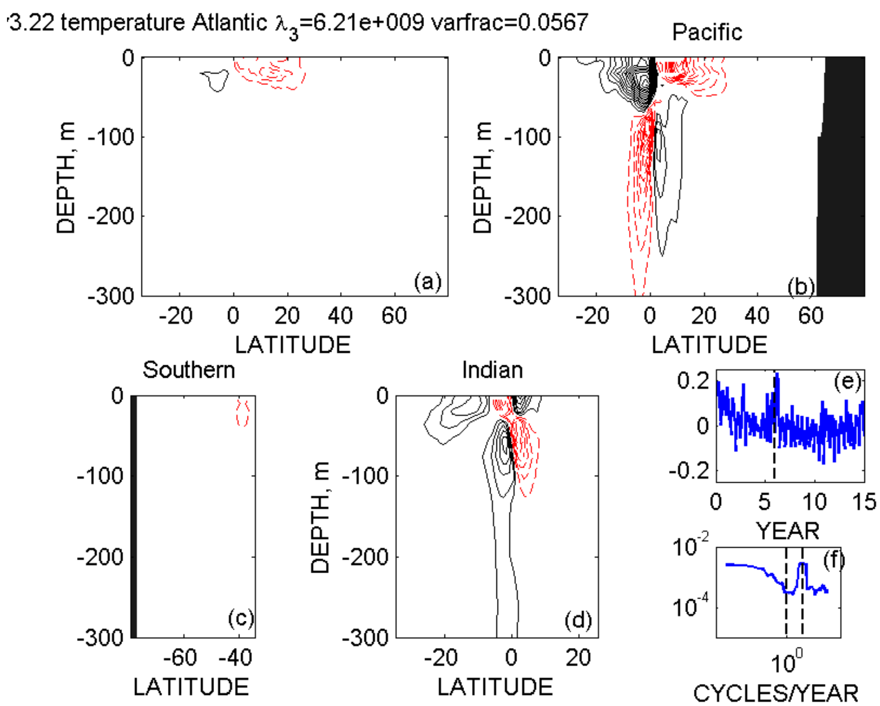

Figure 24: Third EOF of the enthalpy transport, with about 6% of the variance and a dominantly 6 month time-scale. An ENSO signal is again present.

{global_heat_s

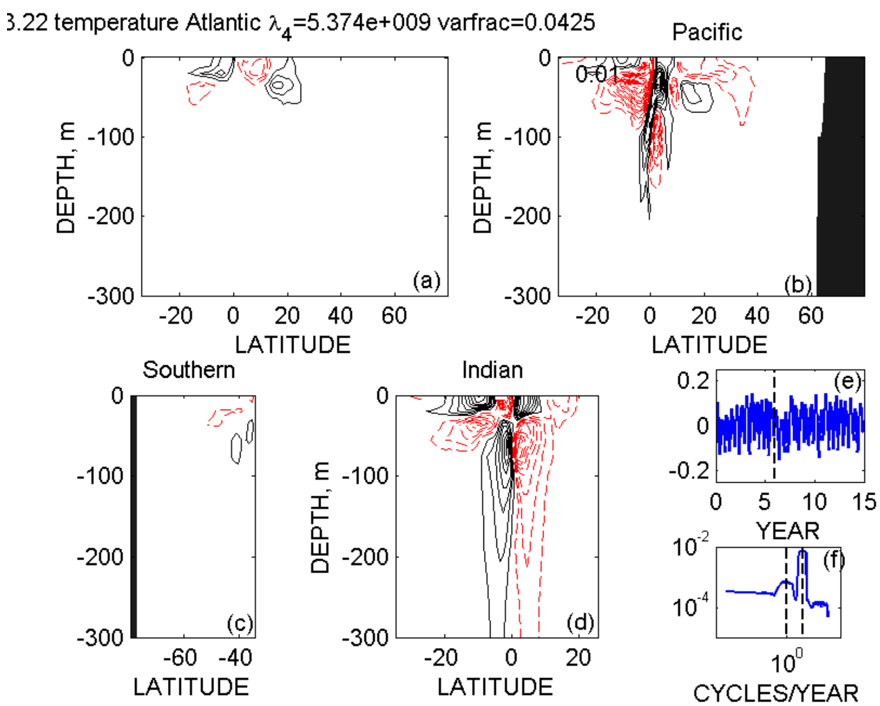

Figure 25: Fourth enthalpy transport EOF with about 4% of the variability variance and again a dominantly 6 month time scale.

{global_heat_s